Statistical prediction of corrosion front penetration

Terje Johnsen[1] and Rudolf Hilfer[1,2,3]
[1]*Department of Physics, University of Oslo, P.O. Box 1048 Blindern, N-0316 Oslo, Norway*
[2]*ICA-1, Universität Stuttgart, 70569 Stuttgart, Germany*
[3]*Institut fur Physik, Universität Mainz, 55099 Mainz, Germany*
(Received 18 September 1996)

A statistical method to predict the stochastic evolution of corrosion fronts has been developed. The method is based on recording material loss and maximum front depth. In this paper we introduce the method and test its applicability. In the absence of experimental data we use simulation data from a three-dimensional corrosion model for this test. The corrosion model simulates localized breakdown of a protective oxide layer, hydrolysis of corrosion product and repassivation of the exposed surface. In the long time limit of the model, pits tend to coalesce. For different model parameters the model reproduces corrosion patterns observed in experiment. The statistical prediction method is based in the theory of stochastic processes. It allows the estimation of conditional probability densities for penetration depth, pitting factor, residual lifetimes, and corrosion rates which are of technological interest. [S1063-651X(97)15805-6]

PACS number(s): 05.40.+j, 82.20.Wt, 81.05.Bx

I. INTRODUCTION

The evolution of corrosion fronts is a complex problem of widespread interest. One distinguishes two different morphologies, uniform corrosion and localized corrosion. Often both morphologies appear simultaneously in the same system. Current interest includes observations of self-affine scaling behavior within localized attacks [1], as well as *in situ* observations of dynamical growth [2] to observations of pit area and depth as function of time [3].

An important scientific and technological question is to predict the lifetime of constructions in different environments. Because of the inherently random character of corrosion, statistical methods such as extreme value statistics are commonly used for such predictions [4,5].

This paper presents a statistical method to predict the evolution of front depths, based on data from experiments or simulations. The basic quantities recorded are the material loss v and maximum depth of front X as functions of time. The evolution process is assumed to be a stochastic process, and the recorded data are used to form probability distributions concerning penetration, lifetimes, corrosion rates, and pitting factors.

Several models have recently been developed for simulation of pitting processes [6,7]. Inspired by these models, we present a three-dimensional (3D) model for pitting corrosion that has been developed from a 2D model [8]. It includes the buildup of an aggressive environment within the pit due to hydrolysis, and transport of aggressive ions as observed in real systems. The patterns obtained by this model look qualitatively similar to real corrosion patterns.

We begin our presentation in Sec. II by explaining our statistical prediction scheme. The scheme is based on the concept of corrosion events and penetration probabilities. Next we describe the simulation model. It simulates a corrosion process with passivation and depassivation. Finally we apply the statistical prediction scheme to the simulation result. We emphasize that the prediction scheme can be applied in the same manner to experimental data.

II. CORROSION EVENTS AND PENETRATION PROBABILITIES

Consider a rectangular piece of material in a corrosive environment inside a box with lateral dimensions L_x and L_y and height L_z. We choose a Cartesian coordinate system whose origin is the left hand corner of the box, and where the x-y plane coincides with the surface of the material.

The volume of material lost by corrosion, $V(t)$, is an increasing function of time. The maximum pit depth is denoted as $X(t)$, and it is defined to be the global minimum in the corrosion front at time t. The total material loss is the integrated volume of material that has been corroded up to time t. The corrosion rate at time t is defined as

$$\gamma(t)=\frac{V(t)}{L_xL_yt}, \tag{1}$$

and it gives the velocity of the corrosion front. The ratio

$$\Pi(t)=\frac{X(t)L_xL_y}{V(t)} \tag{2}$$

is called the pitting factor at time t. The maximum pit depth is a quantitative measure of the localized pitting corrosion processes, while the corrosion rate $\gamma(t)$ characterizes mainly the background or uniform corrosion processes.

The corrosion process is viewed as a time sequence of random corrosion events. An individual corrosion event is defined to occur at an instant t^* if the time derivative $dX(t)/dt$ of the maximum pit depth falls to zero or, in practice, below a small threshold value. This is shown schematically in Fig. 1. For times $t<t^*$ earlier than a corrosion event, the slope $\Delta X(t)/\Delta t$ is larger than the threshold, while for $t>t^*$ it falls below the threshold for at least an infinitesimal time interval. In the jth corrosion event the random variables X, V, and t all increase by random amounts,

$$x_j=X(t^*_{j+1})-X(t^*_j), \tag{3}$$

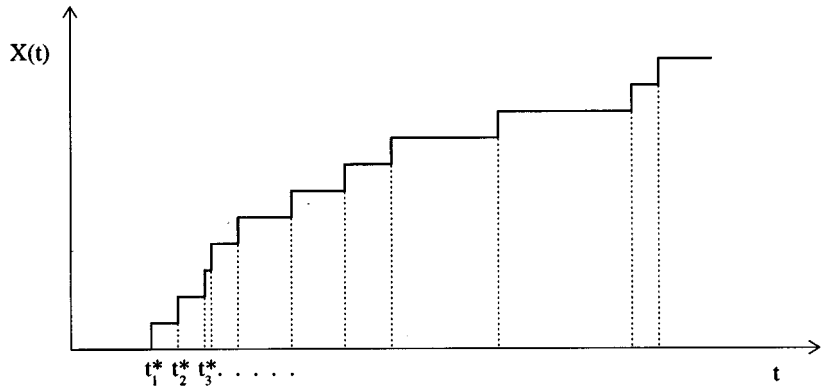

FIG. 1. Illustration of individual corrosion events obtained for a given maximum pit depth $X(t)$ as function of time t. The events are indicated by a dotted line at the time of the event t_j^*.

$$v_j = V(t_{j+1}^*) - V(t_j^*), \tag{4}$$

$$\tau_j = t_{j+1}^* - t_j^*, \tag{5}$$

where $\{t_j^*\}_{j=1,\ldots,M}$ denotes the set of corrosion events. The reaction increments are assumed to be statistically independent, and to have the joint probability density function $w(x,v,\tau)$. The joint probability density function w gives the probability to find the increment of maximum pit depth in the infinitesimal interval $[x,x+dx]$, the material loss increment in the infinitesimal interval $[v,v+dv]$, and the temporal increment in the interval $[\tau,\tau+d\tau]$.

The transition probabilities $w(x,v,\tau)$ are the main input functions for our analysis. They can be determined through observations in the field, through measurements in a laboratory experiment, or through calculations in a simulation. In the present study we use computer simulations to determine $w(x,v,\tau)$ in order to illustrate our approach. Different corrosion processes are characterized and distinguished by different w functions.

The function of main interest is the joint probability density $p(X,V,t)$ that a time t has elapsed and a volume V of material has been corroded when the maximum pit depth reaches the value X given that the corrosive process started at $t=0$ from $X=0$ and $V=0$. This function $p(X,V,t)$ will also be called the penetration probability function, and it forms the basis for the prediction of quantities of interest.

The general theory of stochastic processes allows us to express the penetration probabilities $p(X,V,t)$ in terms of the transition probabilities $w(x,v,\tau)$ [9,10]. The basic relationship reads

$$p(X,V,t) = \frac{1}{i(2\pi)^3}\int_{c-i\infty}^{c+i\infty}\int_{-\infty}^{\infty}\int_{-\infty}^{\infty}\frac{1-\omega(u)}{u[1-w(k_x,k_v,u)]} \times \exp(ut - ik_vV - ik_xX)dk_xdk_vdu. \tag{6}$$

Here

$$w(k_x,k_v,u) = \int_0^{\infty}\int_{-\infty}^{\infty}\int_{-\infty}^{\infty} w(x,v,\tau) \times \exp(ixk_x + ivk_v - u\tau)dxdvd\tau \tag{7}$$

is the Fourier-Laplace transform of $w(x,v,\tau)$, and

$$\omega(u) = \int_0^{\infty}\omega(\tau)e^{-u\tau}d\tau \tag{8}$$

is the Laplace transform of $\omega(\tau)$ where

$$\omega(\tau) = \int_0^{\infty}\int_0^{\infty} w(x,v,\tau)dxdv. \tag{9}$$

For the derivation of Eq. (6) the reader is referred to the literature [10]. The penetration probability $p(X,V,t)$ is completely determined through integrals of the transition probability w. Of course the integrals to be performed cannot generally be calculated analytically, and it may be necessary to resort to numerical methods to evaluate them.

Solution (6) generates predictions for the spatiotemporal behavior of the advancing corrosion front. For a corrosive process in which the transition probability function $w(x,v,\tau)$ has large-t behavior,

$$w(t) \sim t^{-1-\alpha}, \tag{10}$$

with $0<\alpha<1$, it can be shown [10–12] that the width $\xi_{\perp}$ of the advancing corrosion front will grow as

$$\xi_{\perp}(t) \sim t^{\alpha}, \tag{11}$$

and the expected maximum pit depth will increase like

$$\langle X(t)\rangle \sim t^{\alpha} \tag{12}$$

as a function of time. Note that a corrosion process characterized by a transition function w obeying Eq. (10) is strongly intermittent. This means that in such a process there are strong fluctuations in the corrosion rate as a function of time. The temporal fluctuations have the irregular behavior characteristic of fractals in time. Bursts of corrosion activity are separated by quiescent intervals. These quiescent intervals have a fractal distribution of interval lengths with divergent expectation. Thus an average corrosion rate cannot be sensibly defined because it would depend on the length of time over which one averages. Such a behavior is characteristic of some corrosion processes, and Eq. (12) is corroborated by experimental observation [13,5].

We have applied our method to computer simulations where $X(t)$ can be measured directly. In an experiment or field application, measuring this information is also possible. Measuring the transition probability function w directly from

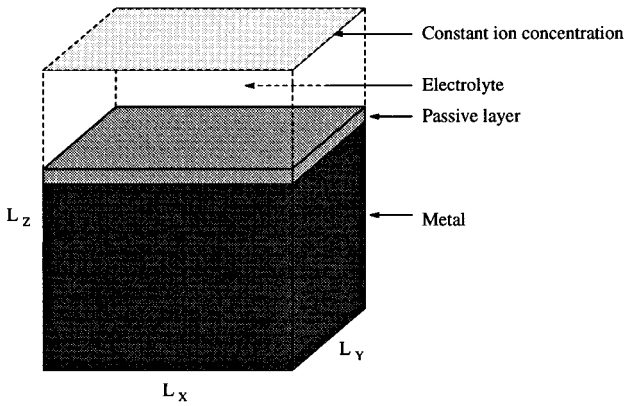

FIG. 2. Simulation lattice consisting of a metal substrate covered with a passive oxide layer. Above the oxide there is an electrolyte region. In the top layer the ion concentration is kept constant.

a computer simulation is particularly convenient for testing the feasibility of our approach.

III. DESCRIPTION OF SIMULATION MODEL

The simulations are performed on a 3D cubic lattice of size $L_x=L_y=256$ and depth $L_z=101$. Periodic boundary conditions are applied in the x and y lateral directions (see Fig. 2). Six different labels will be used to represent the six different states of a lattice site. At the start of a simulation the lattice sites with z coordinates in the range $1\leqslant z\leqslant 89$ represent the uncorroded metal labeled (M). The layer of sites at $z=90$ is given a different label to represent a protective oxide layer (O). Sites in the range $90<z\leqslant 101$ represent the outer aqueous environment. These sites are labeled differently depending on whether they represent cations (C), anions (A) or inert fluid (water or solvent) (U). In the corrosion process, product sites labeled (P) are produced as described below. The cations C, anions A, products P, and inert fluid U are mobile, while M and O are not. At the upper boundary with $z=101$ a constant concentration of A and C is maintained. Figure 2 shows the initial configuration of the simulated system.

A simple move of the simulation consists in choosing one site S occupied by a movable ion A, C, or P and trying to move it onto a nearest neighbor target site using force biased transition probabilities. Whether or not the attempted move is successful depends on the occupation of the target sites.

To choose a target site for a force biased move, neighboring sites are inspected within a region K of $5\times5\times5$ lattice units defined as

$$K=\{|\vec{r}_{0,j}-\vec{r}_j|\leqslant 2, j=x,y,z\}, \tag{13}$$

where $\vec{r}_{0,j}$ is the chosen site S from which the move starts. K can be considered as the union of six pyramidic shaped regions,

$$K=K_x^{\pm}\cup K_y^{\pm}\cup K_z^{\pm}. \tag{14}$$

The particles in each region $K_j^{\pm}$ are assumed to exert a net force in the j direction on the particle at site S. Charges of $Z_A=-1$, $Z_C=1$, and $Z_P=2$ are associated with sites labeled A, C, and P, respectively. The net force in the positive x direction is

$$F_x^{+}=A\left(\sum_{i\in K_x^{+}}\frac{Z_S Z_i}{r_i^2}-\sum_{i\in K_x^{-}}\frac{Z_S Z_i}{r_i^2}\right), \tag{15}$$

where A is a constant, Z_i is the charge value, and r_i is the Euclidean distance to site S. Analogously the forces in the y and z directions are obtained from charges in the volumes $K_y^{\pm}$ and $K_z^{\pm}$.

To calculate the transition rates, we view the ion motion as an activated process. The net force on S gives rise to unequal transition rates [14]. The transition rate k_j for a move in the j direction is

$$k_j=e^{BF_j l}, \tag{16}$$

where $j=x^{\pm},y^{\pm},z^{\pm}$, B is a constant, and l is the step distance. The constants were set to $ABl=1$ for the simulations discussed here. The rates are calculated for all six possible move directions, and the sum of the rates is

$$k_{all}=\sum_{j=1}^{6}k_j. \tag{17}$$

The target site $T(S)$ is selected among the six directions by drawing a random number Ξ in the interval $[0,k_{all}]$. The direction j is chosen if

$$\sum_{i=0}^{j-1}k_i<\Xi\leqslant\sum_{i=0}^{j}k_i, \tag{18}$$

i.e., if the reaction rate k_j falls in the corresponding subinterval. $T(S)$ is then selected as the nearest neighboring site in the direction j.

The time is incremented by one unit every $N_d=N_A+N_C+N_P$ moves, where $N_A(t)$, $N_C(t)$, and $N_P(t)$ are the number of A, C, and P sites, and $N_d(t)$ is the total number of movable sites. In other words, the time step is

$$\Delta t=\frac{1}{N_d}. \tag{19}$$

If an ion within the layer $z=100$ steps onto the layer at $z=101$, it is removed from the simulation. Simultaneously, new ions enter the lattice from the layer at $z=101$ at a rate that depends on the constant ion concentration and the force exerted from nearby ions.

The A and C ions are initially positioned at random in the region for $90<z\leqslant 100$. The protective oxide layer at $z=90$ covers the metal completely. The immobile sites O in the oxide layer can react and form a mobile corrosion product P. This reaction $O\rightarrow P$ exposes bare metal sites that can later dissolve into the aqueous phase. The exposed metal can react to form product $M\rightarrow P$ or oxide $M\rightarrow O$. In this way the number N_b of bare metal sites change continually during the simulation of the corrosion process.

A flow diagram of the main program loop in our simulation is shown in Fig. 3. The monomolecular dissolution $M\rightarrow P$ and passivation reactions $M\rightarrow O$ appear in A and B.

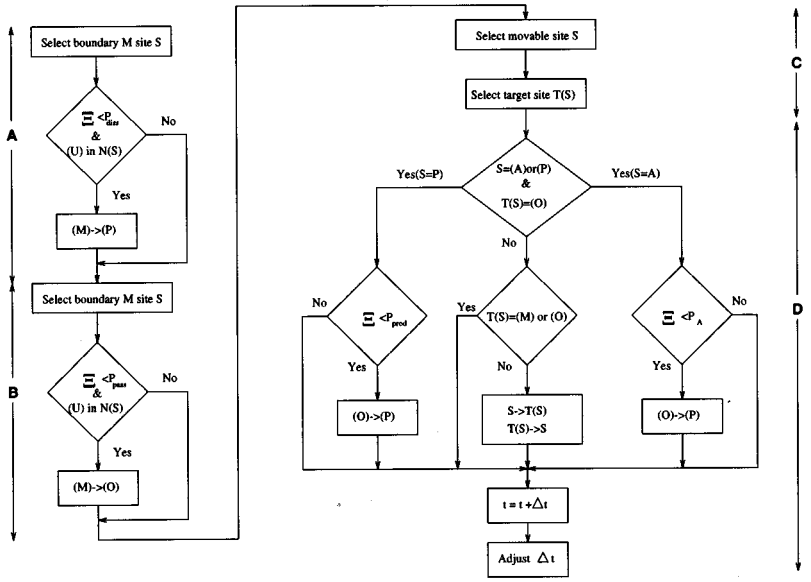

FIG. 3. Flow diagram of the main loop of the program executed in a time interval Δt in the simulation. The label S means a selected site. $N(S)$ represent the set of six nearest neighboring sites, and $T(S)$ means the target site of a selected move. The variable Ξ represents a uniformly distributed random number.

The schematic representation of the adjacent sections A and B read as follows: First a metal site at the boundary of the aqueous phase is drawn at random. A boundary site is a site not surrounded entirely by other M or O sites. The dissolution probability P_{diss} of the boundary site is given by

$$P_{\mathrm{diss}}=k_{\mathrm{diss}}N_b\Delta t=\frac{k_{\mathrm{diss}}N_b}{N_d}, \tag{20}$$

where k_{diss} is a reaction rate constant. A random number $0\leqslant\Xi\leqslant 1$ is drawn from a uniform distribution. If $\Xi<P_{\mathrm{diss}}$ and there exists a nearest neighbor labeled U, the metal dissolves, $M\rightarrow P$. If not proceed to section B. Section B is analogous to section A, with the passivation probability P_{pass} given as

$$P_{\mathrm{pass}}=k_{\mathrm{pass}}N_b\Delta t=\frac{k_{\mathrm{pass}}N_b}{N_d}, \tag{21}$$

where k_{pass} is a reaction rate constant.

In section C a site occupied by anion A, cation C, or product P is selected at random. For the selected site S a target site $T(S)$ is determined as described above. Depending upon the state of S and $T(S)$ three different choices are allowed in section D of Fig. 3. If $T(S)\neq O$ or $S=C$, the middle path is selected. If further $T(S)=M$ or $T(S)=O$ no move takes place. If $T(S)\neq M$ or $T(S)\neq O$ the particles at sites S and $T(S)$ are interchanged. The two paths of the flow diagram in section D to the left and right are analogous in structure, and are discussed together. If site $S=A$ (right) or $S=P$ (left) and $T(S)=O$, these paths are selected. A reaction is initiated given the condition $\Xi<P_{\mathrm{prod}}$ or $\Xi<P_A$, respectively, where P_{prod} and P_A are probability constants. This transforms an oxide site into a product site, $O\rightarrow P$. In the end of section D the time t and time interval Δt are updated before the loop returns to the start of section A.

Having described our simulation algorithm we now discuss the physical-chemical processes underlying the simulated model. Mass transport in our model is purely diffusive. The charged nature of ions is modeled through a bias in the diffusion, and hydrodynamic flow is neglected.

A metal in contact with a corroding environment is often covered by an oxide layer [15], which in our model is represented by O. Various mechanical and chemical reactions can destroy the integrity of the layer locally. In our model we consider chemical oxide destruction represented by the reaction $A+O\rightarrow A+P$. A common example from the literature are Cl^- ions for a range of metals and alloys, i.e., Ni, Al, and stainless steel [15,16]. In the model, anions are given a probability P_A to convert an oxide site into a corrosion product P. The cations C are assumed unreactive.

As bare metal sites are exposed, metal dissolves with a rate constant k_{diss} according to the reaction

$$M\Rightarrow M^{n+}+ne^-, \tag{22}$$

where $n=2$ in our model. This charge released to the bulk metal in a dissolution process must be consumed either by an external connection or by cathodic reactions in a real metal system. In the model the cathodic part of the corrosion process is taken to be fast and not to limit the dissolution rate. The actual cathodic reaction is not modeled.

In many corrosion processes the metal ions react with water to form metal hydroxides and hydronium ions [17,18] in the reaction

$$M^{2+}+4\mathrm{H_2O}\Leftrightarrow M(\mathrm{OH})_2+2\mathrm{H_3O}^+. \tag{23}$$

Product sites P in the model can be considered to represent both metal ions from reaction (22) and the further hydrolysis products from Eq. (23). The increasing acidity destabilizes the oxide sites [19]. A probability P_{prod} to remove oxide sites by contact with product sites is therefore included. The model does not include formation of salts which affect the dissolution rate. Instead, if the nearest neighbor shell of a metal site does not contain solvent U, the dissolution process is postponed until a more dilute electrolyte results. The concentrated environment without solvent is also believed to have a low pH due to hydrolysis reactions of metal ions, and this reduces the formation of oxide sites. This is imple-

TABLE I. Simulation parameters.

Run No.	k_{diss}	k_{pass}	P_{prod}	P_A	C_0
R_1	10^{-2}	5×10^{-3}	10^{-2}	10^{-4}	25%
R_2	10^{-2}	10^{-2}	10^{-4}	10^{-4}	25%

mented as the condition of requiring at least one U site at nearest neighbor position for a passivation process to occur. The detailed processes involved in oxide breakdown and formation are not represented in the model.

In addition to the two processes of oxide destruction, fresh oxide is created at bare metal sites with rate constant k_{pass}. The initial electrolyte represents a salt which is assumed to have dissociated completely into ions, such as Na^+Cl^-. Outside the simulated lattice at $z>101$ a constant concentration bulk electrolyte is maintained. Ions which enter this region from the region $z<100$ are removed by the flow. All ions are subject to both diffusion and interactions. In the model a simplified Coulomb interaction of ions within a given volume of $5\times5\times5$ lattice sites has been included as described above. This perturbs the free diffusion and increases the concentration of anions within a pit above the bulk concentration. The effect is known experimentally [20,21] to increase the corrosivity within the pit, and it reduces the probability of pit repassivation.

The model requires the parameters k_{diss}, k_{pass}, P_{prod}, and P_A together with the bulk electrolyte concentration C_0 as input. In the simulations we used two different sets of parameter values which are listed in Table I. Cross sections of the resulting corrosion patterns are shown in Fig. 4. The images on the left show smoother fronts than the rough pits to the right. The black sites mainly observed within the rougher pit are passive sites that form complex diffusion paths for the movable ions. The simulations were terminated at a maximum pit depth of 22 lattice units for R_1 (left) and 20 lattice units for R_2 (right).

The metal sites in the present model consisted of equal labeled sites with equal reaction rates. To include impurities or alloys in the model additional sites with additional labels could be included in a future improvement. This would allow us to assign different reaction rates leading to preferred sites for pit initiation.

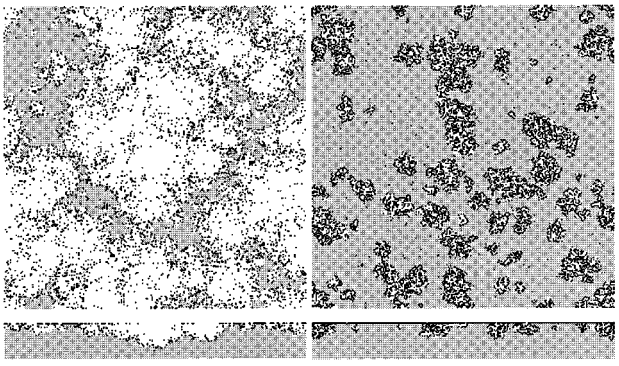

FIG. 4. Cross section in the x-y plane (top) and x-z plane (bottom) for patterns produced by two different sets of parameters R_1 (left) and R_2 (right). Light gray represents uncorroded metal sites, and black sites are passive oxide sites. Passive or metal sites disconnected from the base of the metal in the process are not removed. The left image shows a corroded volume with a more open smooth surface than the structure seen to the right.

Changes in the electrochemical potential as a result of localized corrosion processes are known to influence the reaction rates locally [22]. Difficulties arising from such effects are not included in this version of the model, but are left for future refined models.

IV. APPLICATION OF THE PREDICTION SCHEME TO THE SIMULATION DATA

A. General definitions

In this section we apply the prediction scheme described in Sec. II to predict the maximum pit depth, pitting factor, lifetime, and corrosion rate for the model described in Sec. III. The predictions could in principle be calculated from experimental data. To this end it is necessary to measure the corroded volume from iron counts or weight loss measurements together with identifications of maximum pit depths as a function of time.

To apply the method to our computer simulations we record the integrated material loss and the elapsed time whenever the maximum pit depth increases by one lattice unit. This increase of $X(t^*_{j+1})-X(t^*_j)=1$ represents a corrosion event in the simulation. Thus instead of measuring $X(t)$ and $V(t)$ directly the inverse functions $t(X(t^*_j))$ and $V(X(t^*_j))$ were recorded. The differences x, v, and τ were calculated according to Eqs. (3)–(5), and collected into a histogram approximating the transition probability function $w(x,v,\tau)$. Based on this approximation the penetration probability $p(X,V,t)$ could be calculated numerically.

The penetration probability $p(X,V,t)$ allows us to obtain quantities of great interest. A typical question that can be answered is the following: What is the probability of finding a maximum pit depth X if it is known that the material was immersed in a corrosive environment for a time t, and that within this period a total material loss $V(t)$ has accumulated? Such a conditional probability density $p(X|V,t)$ for the maximum pit depth given the material loss and the elapsed time can be calculated from the penetration probability function $p(X,V,t)$ as

$$p(X|V,t)=\frac{p(X,V,t)}{p(V,t)}, \tag{24}$$

where

$$p(V,t)=\int_{-\infty}^{\infty}p(X,V,t)dX. \tag{25}$$

Similarly the probability density for a sample of thickness X to have lifetime t is obtained as $p(t|X)$ after integrating out the material loss. This conditional lifetime probability density gives the distribution of lifetimes (i.e., the time before failure) of a material with wall thickness X. Residual lifetimes can also be estimated given the remaining wall thickness.

The time dependent probability density for the pitting factor $p(\Pi|V,t)$, given the material loss where Π is defined in Eq. (2), and the distribution of corrosion rates $p(\gamma|X,V)$, as

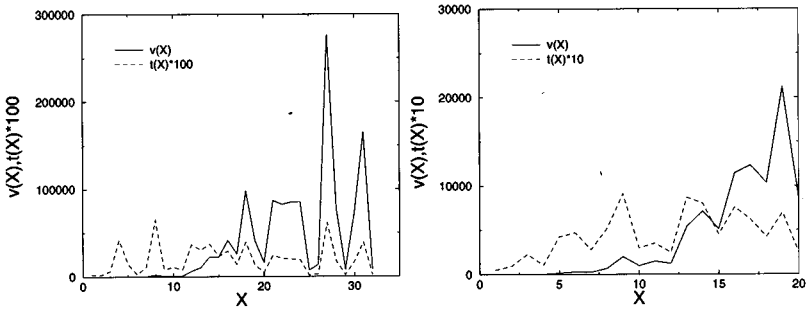

FIG. 5. The increments $v(X)$, number of lattice sites removed, and $t(X)$, elapsed time steps, as a function of maximum pit depth X measured in lattice units where run parameters R_1 and R_2 are used for the left and right plots, respectively. The data for $t(X)$ were multiplied by factors of 100 (left) and 10 (right) for better visualization.

defined in Eq. (1), have also been calculated. The penetration probability distributions could in principle be estimated directly from our computer simulations. However, to obtain adequate statistics on the order of 10 000, such runs would have to be performed. With present technology, such extreme calculations are only possible for very small systems. For our systems of size $256\times256\times100$ lattice units, only a small number of runs are feasible. Our prediction method allows us to extrapolate the results to much larger systems.

B. Specific results

Measurements of the increments v and t during corrosion events as a function of maximum pit depth X are plotted in Fig. 5. The left plot was obtained by use of the parameters R_1, and the right plot by R_2. The run R_1 stops at depth $X=22$. To assess the influence of transients the R_1 run was resumed, and extended to a depth $X=32$. The extended run is referenced as $R_{1,\mathrm{Ext}}$.

The volume increment $v(X)$ shows an increasing trend for both simulations whereas the time increments $t(X)$ tend to fluctuate without a systematic trend. The transient is most pronounced in the early stage of the left plot, whereas the remaining part indicates a stationary behavior. The initial increase in $v(X)$ can be understood from the approximately hemispherical form of the early pits. Between two corrosion events the radius of the pit increases on the average by one lattice unit, which results in a steady increase in v. Additional pits are initiated elsewhere at the top surface, increasing v even more. This transient behavior will be dominant as long as the pits grow separately. At a later stage pits combine, as can be observed to the left in Fig. 4. At the end of run $R_{1,\mathrm{Ext}}$ all pits have combined, and the transient behavior has turned into a continuous growth, characteristic of uniform corrosion.

From the functions $v(X)$ and $t(X)$ it is possible to estimate the transition probabilities $w(x,v,\tau)$. The transition probability function $w(x,v,\tau)$ is then used to estimate the conditional probability densities. Random τ and v increments are drawn from $w(x,v,\tau)$ and accumulated. To estimate $p(X|V,t)$ the accumulation of random increments is continued until the accumulated volume falls into the interval $[V_{\min},V_{\max}]$ and the accumulated time into the interval $[t_{\min},t_{\max}]$, where

$$V_{\max}=V+f\overline{v},\quad V_{\min}=V-f\overline{v},$$
$$t_{\max}=t+f\overline{\tau},\quad t_{\min}=t-f\overline{\tau}. \tag{26}$$

Here f is a parameter, and $\overline{v}$ and $\overline{\tau}$ are the average increments.

1. Distributions for run R_1 and $R_{1,Ext}$

Figure 6 shows the predicted conditional probability densities for runs R_1 and $R_{1,\mathrm{Ext}}$. These predictions were made from the histograms, given the condition that V and t have the same values as were actually observed at the end of the simulation runs, see legend of plot (A), with $f=1$. The solid curve results from the simulation run R_1 and the dashed curve is from run $R_{1,\mathrm{Ext}}$. The conditional probability density for the maximum pit depth, $p(X|V,t)$, shown in (A) indicates a maximum probability in the region of the termination depth of the runs, as expected. The extended run has a somewhat wider distribution, which reflects the large fluctuations observed in the later stage of the simulation as shown in the left plot of Fig. 5. Plot (B) in Fig. 6 shows that the predicted pitting factor decreases as more and more pits coalesce in the extended run. The predicted lifetimes in plot (C) follow the termination times and corrosion rates in (D), indicating an increased predicted rate as the run is extended.

2. Dependence on conditions and condition intervals

To explore the usefulness of these predictions it was studied how the predictions depend on the conditions and the interval that was specified for the conditions. The left side of Fig. 7 shows conditional probability distributions $p(X|V,t)$ for a maximum depth obtained from the R_1 histogram by use of different conditional parameter intervals with f in the range $f=[0.5,5]$. The solid unmarked curve with $f=5$ will predict a lower value for the maximum depth, as expected from its low value of $V_{\min}$ and $t_{\min}$. When f is lowered, the interval decreases and a smaller fraction of the iterations are successful. This results in poorer data quality of the predictions, and requires more computations for the same data quality. From the plot one sees that the maximum probable depth that is predicted approaches the termination depth $X=22$ with decreasing f.

To illustrate the effect of transients in the basic quantity $p(X|V,t)$, we have plotted to the right in Fig. 7 the maximum pit depth probability functions for the R_1 (solid curve) and $R_{1,\mathrm{Ext}}$ (dashed curve) histograms given the conditions $V_{R_{1,\mathrm{Ext}}}$ and $t_{R_{1,\mathrm{Ext}}}$ at the termination stage of the extended run with $f=2$. The two curves differ as a result of the transient behavior of the volume increments. The R_1 histogram curve oversamples increments from the transient region relative to the extended run. Increments from the transient region are

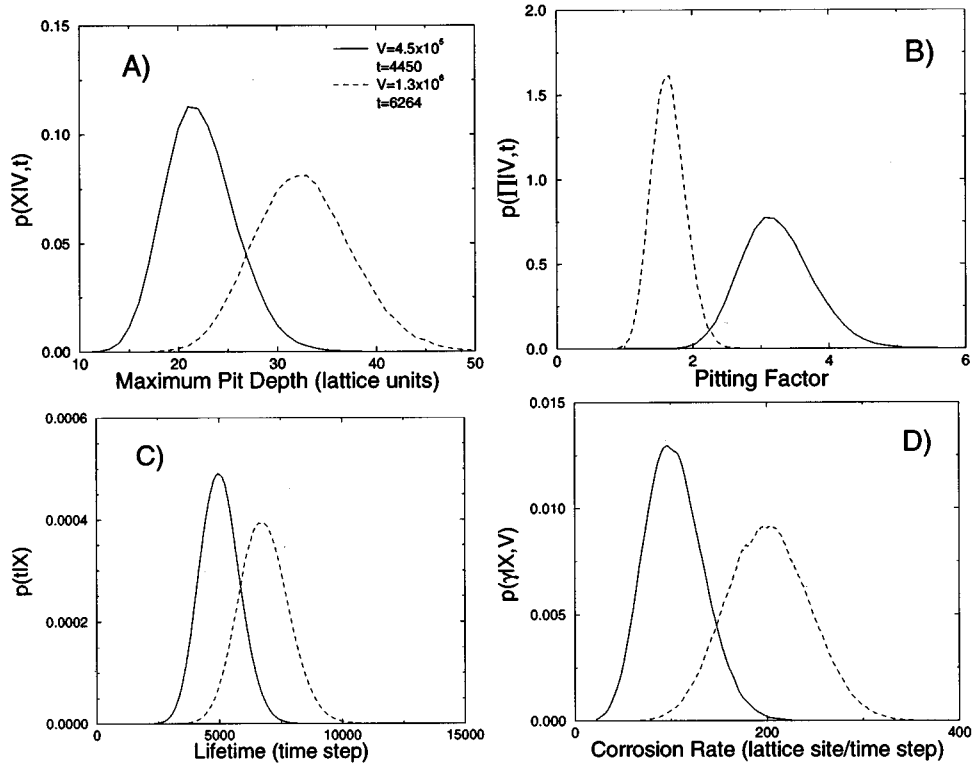

FIG. 6. Conditional penetration probabilities (A), pitting factor probabilities (B), lifetime probabilities (C), and corrosion rate probabilities (D) have been calculated for simulation run R_1 ($X=22$) drawn with a solid curve, and the extended run $R_{1,\mathrm{Ext}}$ ($X=32$) drawn with a dashed curve. The final mass loss and final elapsed time used for estimating the conditional probabilities for the two runs are listed in the legend of the plot labeled (A).

small and will therefore lead to a faster penetration for the R_1 histogram.

Figure 8 shows $X_{\max}$ versus the conditional parameter V, where $X_{\max}$ is the X value corresponding to the maximum of $p(X|V,t)$. The most probable pit depth, $X_{\max}$, was plotted for different conditions V for the R_1 and $R_{1,\mathrm{Ext}}$ run. A relatively small number of iterations, $N=10.000$, were used in these calculations. The conditions were set to $V=V_{R_1}+nf\overline{v}$ and $t=t_{R_1}+nf\overline{\tau}$, where n is a positive integer, $f=1$, and V_{R_1} and t_{R_1} represents the termination values of the R_1 simulation. A plot of $X_{\max}$ versus the conditional parameter t would show similar behavior. This indicates that predictions of maximum pit depths based on iron counts are higher for short runs (R_1) than for longer runs ($R_{1,\mathrm{Ext}}$). Hence short runs with large transients lead to a more conservative prediction.

In Fig. 9 the most probable pit depth $X_{\max}$ has been plotted for different combinations of conditional parameters V and t. One of the conditions were held constant while the other was allowed to change. The constant conditional parameter was set to $V=6V_{R_1}$ and $t=6t_{R_1}$ for the calculations in the left and right side plots, respectively. For each combination (V,t), $N=120.000$ iterations were performed to calculate the histogram. For combinations of (V,t) that were unlikely to be observed, the procedure terminated with zero or very few iterations fulfilling the conditions. The number of iterations was here too small, leading to difficulties when identifying $X_{\max}$. Wide spreading of $X_{\max}$ was observed in

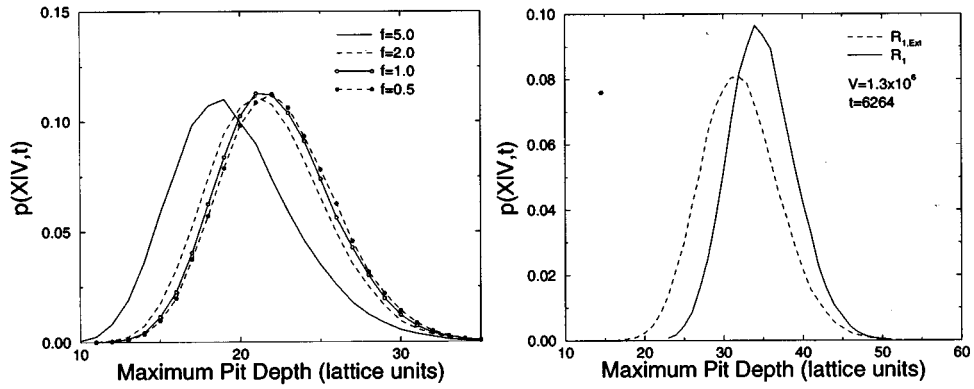

FIG. 7. Left: Conditional penetration probability given conditions from the end of simulation R_1 (V_{R_1},t_{R_1}) with variations of the conditional parameter interval specified by f as listed in the legend. Right: Comparison of the predictions made from the two histograms R_1 and $R_{1,\mathrm{Ext}}$, given the conditions at the termination stage of run $R_{1,\mathrm{Ext}}$ as listed in the legend.

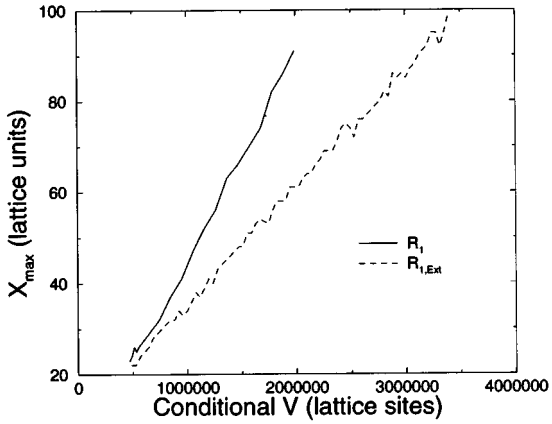

FIG. 8. The most probable depth $X_{\max}$ found at $\max[p(X|V,t)]$ is plotted given different combinations of conditional material loss V and time t. The solid curve represent results from the R_1 simulation histogram and the dashed curve is from the extended run. The conditions V and t were increased by adding integer number of $\overline{v}$ and $\overline{\tau}$, starting at the conditions given at the termination of simulation run R_1. The conditional parameter intervals were set by the parameter $f=1$.

the outer part of the varying condition parameter range, as observed most clearly in the right plot. This is ascribed to the effect of a scarcely populated histogram. The spread in $X_{\max}$ along the axis of the free parameter is ≈ 10 in both plots for the $R_{1,\mathrm{Ext}}$ run and somewhat smaller for the shorter run. The actual increase in the left plot (constant V) and the more steady behavior in the right plot (constant t) probably relates to the specific positions in the parameter space and the form of the histogram used. Parameters in other regions would result in a different appearance.

The range of where parameter settings resulted in fulfillment in the numerical procedure shows that the two histograms are different. What is observed is that, given one condition, two limiting values of the other condition can be estimated from the plot. In principle, maps of the limiting conditional parameters could be estimated from a series of similar calculations, given an iteration number N.

In general, we can conclude that an accumulated histogram with an initial transient in the increments consisting of small values, will predict a too large maximum probable depth if the conditions are set above the end values of the histogram accumulated runs. This gives a conservative prediction. Too low a predicted maximum depth will result if the conditions are set below the end values. This is due to oversampling and undersampling of the transient increments.

If the transient period of the increments is small compared to the whole data set, its effect on the probability predictions is less significant than in our case, where it extends over a longer period. Often the whole set of increments can be treated as one randomly fluctuating set.

If the process generates increments that have a transient character which influence the predictions in a significant manner, special attention must be paid to handle this in a proper way. One way to incorporate these initial increments would be to identify a typical depth X_{trans} where the transient region ends. Increments that belong to different maximum pit depths $X_i < X_{\mathrm{trans}}$ are then collected into separate histograms $w_i(x,v,\tau)$. Increments found at $X > X_{\mathrm{trans}}$ contribute to the ordinary histogram $w(x,v,\tau)$. When calculating the conditional probabilities numerically, one value is drawn initially from each histogram in the depth interval $X=1$ to X_{trans}. This is followed by randomly selecting increments from $w(x,v,\tau)$ until the condition is met. A large number of iterations by use of this procedure produces the probability distributions given the condition. In addition to the maximum probable depth, the width of the distributions are important, indicating the uncertainty of the prediction.

3. Distributions for different simulation parameters

Figure 10 shows the predicted conditional probability densities for the two different sets of parameters R_1 and R_2 of Table I. The predictions were made from the histograms given the condition that V and t have the values observed at the end of the simulation runs as listed in the legend of plot (A). The interval was set to $f=1$. The solid curve results from the simulation run R_1 and the dashed curve from run R_2. The maximum pit depth probabilities of the two simulations show almost similar behavior as expected from their termination depths of $X=22$ and 20. All other predictions however are different. The large difference in the pitting factor reflects a morphology of the R_1 pattern that is close to

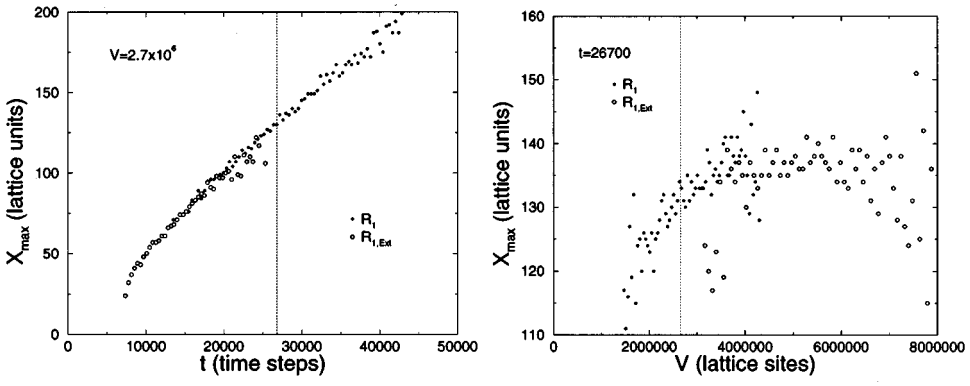

FIG. 9. This plot shows the most probable depth $X_{\max}$ found at $\max[p(X|V,t)]$, given different combinations of conditional material loss V and time t by use of the R_1 and $R_{1,\mathrm{Ext}}$ run histograms. V and t are held constant in the left and right plots, respectively, whereas the other parameter is allowed to change. The dotted line indicates where the constant value was set for the other plot.

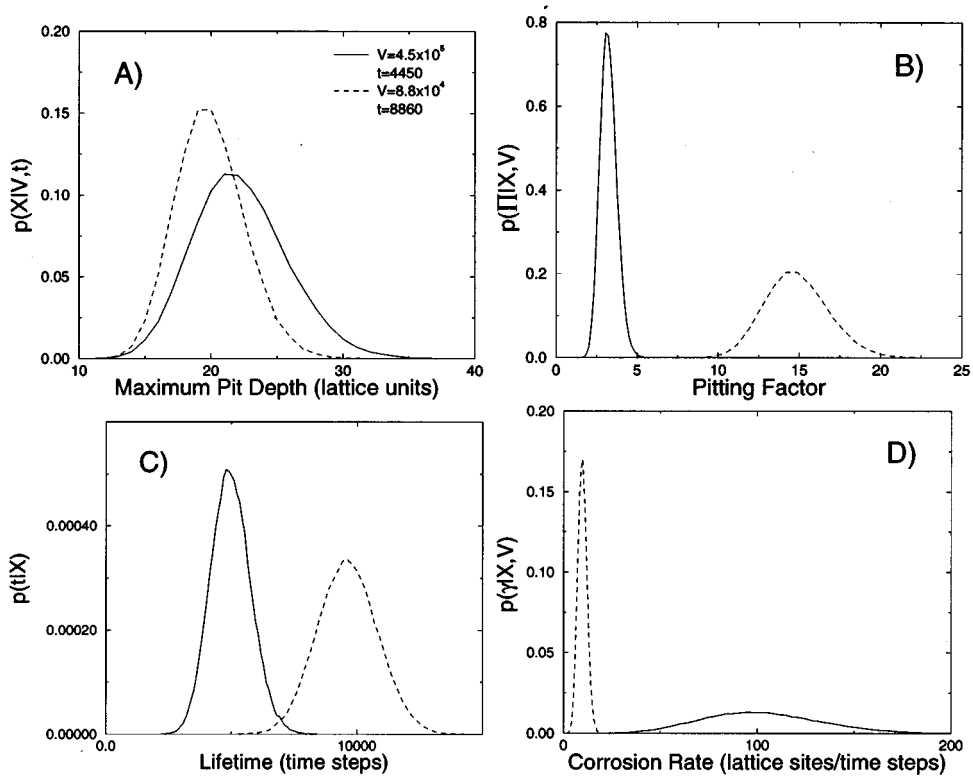

FIG. 10. The solid curve shows run R_1, and the dashed curve represents a simulation run with parameters R_2. The conditional parameters V and t that were used are listed in the legend of plot (A). These values correspond to the final stage of the simulations. (A) This plot shows the probability of reaching a given maximum depth with conditional information from material loss V and time t. (B) Conditional pitting factor probability given the final material loss. (C) This plot shows the probability for a material of given wall thickness (22 for R_1 and 20 for R_2) to last for a certain time. (D) Conditional corrosion rate probability given the wall thickness of the R_1 and R_2 simulations.

uniform corrosion, whereas the large value of R_2 indicates a heavily pitted morphology. This agrees with the morphology shown in Fig. 4. Note, however, that the pitting factor alone can be misleading if it is used to predict internal pit morphology. If the morphology consists of only one pit, a higher pitting factor could indicate a rougher pit or a deeper pit relative to a smooth hemispherical formed pit at the same maximum depth. Both shapes would lead to a higher pitting factor.

Lifetime predictions indicate approximately twice as long lifetime for R_2 versus the R_1 run. The difference of termination depth, $X=22$ for R_1 and $X=20$ for R_2, does not account for the large lifetime difference. The longer lifetime of R_2 can be understood from the simulation parameters. R_2 has twice as high a passivation rate as compared to R_1, and will therefore more easily form protection against further dissolution. At the same time, corrosion products in the R_1 run were assumed to be 100 times more aggressive toward passive sites than in the R_2 run. The surface of R_2 pits therefore has a higher coverage of passive sites, leading to slower growth speed. The predicted corrosion rate for R_2 is small compared to R_1. This was expected from the high pitting factor and long lifetime prediction of R_2.

V. CONCLUSION

A statistical method has been developed to predict the evolution of front depths based on information of the material loss V and maximum depth of front X as a function of time t. The statistical method was applied to our developed 3D model of corrosion. The model includes local breakdown of a protective layer in a simulated aggressive environment forming localized attacks (pits) with an aggressive local environment due to hydrolysis of corrosion products and anion concentration buildup that resist repassivation. Several of these pits grow and eventually combine to form a more complex corrosion front that is qualitatively similar to many real corrosion patterns. This long time limit represents a front that can be characterized as uniform corrosion or a mixture of uniform and pitting corrosion. From the accumulated transition probabilities $w(x,v,\tau)$ obtained from the simulation model, conditional probability distributions were estimated for the penetration depth, pitting factor, lifetime, and corrosion rate.

We observed that a conservative prediction resulted in the case when the histogram is influenced by transients. This conservative estimate converges to the stationary situation when the accumulation time was increased. When there is no transient in the increments, the accumulation range should not cause large changes to the predictions. An alternative method of collecting increments from transient and nontransient regions into different histograms was suggested.

Conditional parameter settings and their interval specified by f influenced the prediction of penetration depth. Different limits of where penetration depths could be estimated given a number N of iterations can be found from calculations using

varying conditional parameters. Such calculations identify regions in (V,t) space that are most likely to be observed. We found by one example that the R_1 run and the extended simulation resulted in different prediction regions as a result of the transient.

The difference between the pitted morphology of run R_2 and the more uniform corrosion pattern of run R_1 can be clearly distinguished from the conditional probability densities of the pitting factor. This shows that our method is useful to determine the morphology of the corrosion pattern. Finally, we emphasize again that the same statistical predictions presented here for simulation data can be applied in the same manner to increments measured in an experiment.

ACKNOWLEDGMENTS

We thank Mike W. Joosten, Conoco Inc., for his discussions and his enthusiastic interested support. T.J. acknowledges the helpful discussions with Paul Meakin and Torstein Jøssang in the model development. We are grateful to Conoco Inc., Fracton A/S, Norsk Hydro, and the Norwegian Research Council (NFR) for financial support and grant of computing time (NFR).

[1] M. W. Joosten *et al.*, *Fractal Behavior of CO_2 Pits, Corrosion/92*, NACE Report No. 11, 1992.
[2] M. W. Joosten *et al.*, *In Situ Observation of Localized CO_2 Corrosion, Corrosion/94*, NACE Report No. 3, 1994.
[3] R. Pierpoline *et al.*, in *Advances in Localized Corrosion*, edited by H. S. Isaacs, U. Bertocci, J. Kruger, and S. Smialowska (NACE, Houston, 1987), pp. 123–126.
[4] H. F. Finley, *Corrosion*, NACE Report No. 83, 1967.
[5] P. Laycock, R. Cottis, and P. Scarf, J. Electrochem. Soc. **137**, 64 (1990).
[6] T. Nagatani, Phys. Rev. Lett **68**, 1616 (1992).
[7] P. Meakin, T. Jøssang, and J. Feder, Phys. Rev. E **48**, 2906 (1993).
[8] T. Johnsen, A. Jøssang, T. Jøssang, and P. Meakin (unpublished).
[9] R. Iranpour and P. Chacon, *Basic Stochastic Processes, The Mark Kac Lectures* (McMillan, New York, 1988).
[10] E. W. Montroll and B. J. West, in *Fluctuation Phenomena*, edited by E. W. Montroll and J. L. Lebowitz (North-Holland, Amsterdam, 1979), p. 61.
[11] R. Hilfer and L. Anton, Phys. Rev. E **51**, R 848 (1995).
[12] R. Hilfer, Fractals **3**, 211 (1995).
[13] R. Hausler and P. Burke, Report No. 26, NACE, 1985 (unpublished).
[14] J. O. Bockris and A. K. N. Reddy, *Modern Electrochemistry 1* (Plenum, New York, 1970).
[15] Z. Szklarska-Smialowska, *Pitting Corrosion of Metals* (NACE, Houston, TX, 1986).
[16] T. P. Hoar and W. R. Jacob, Nature **216**, 1299 (1967).
[17] M. Pourbaix, in *Localized Corrosion*, edited by R. W. Staehle, B. F. Brown, J. Kruger, and A. Agrawal (NACE, Houston, 1974), pp. 12–33.
[18] K. P. Wong and R. C. Alkire, J. Electrochem. Soc. **137**, 3010 (1990).
[19] M. Pourbaix, *Atlas of Electrochemical Equilibria in Aqueous Solutions* (Pergamon, Oxford, 1966).
[20] T. Suzuki, M. Yamabe, and Y. Kitamura, Corrosion **29**, 18 (1973).
[21] J. Mankowski and Z. Szklarska-Smialowska, Corrosion Sci. **15**, 493 (1975).
[22] H. S. Isaacs and M. W. Kendig, Corrosion **36**, 269 (1980).